ADVANCED MATERIALS INTERFACES
www.advmatinterfaces.de

Nanoscale Molecular Building Blocks for Layer-by-Layer Assembly

*Shinyoung Choi, Nguyen Ngan Nguyen, Yangjin Lee, Seong-Jun Yang, Kwanpyo Kim, Kilwon Cho, and Cheol-Joo Kim**

Ultrathin molecular films can be used as building blocks to enable rational design of functionalities at the molecular level. A versatile and scalable approach to fabricate transfer-compatible ultrathin molecular films with a broad range of physiochemical properties is reported. Different molecules in layers of uniform nanoscale thickness are deposited on monolayer hexagonal boron nitride (ML h-BN) film. Initially, the deposited molecules form islands due to limited molecular diffusion during deposition on ML h-BN, but postannealing effectively transforms them to the thermodynamically preferred film structures. Ultrathin building blocks composed of ML h-BN and different molecules (C_{60}, pentacene, $C_{44}H_{32}N_2$) are realized, then transferred layer-by-layer (*L*-by-*L*) to form materials with precisely controlled composition and thickness, including donor/acceptor superlattices. This approach can facilitate the integration of nanoscale molecules with different material platforms for advanced functionalities.

1. Introduction

Organic molecules have a broad range of physiochemical properties, which are determined by molecular shape, orbital energy, and chemical reactivity. Integration of single or multiple molecules with various devices forms the basis for many applications, including (opto-)electronics, energy devices and chemical sensors.[1] A technique to control the thickness and composition of organic building blocks at the molecular scale could provide a powerful way to design materials with previously inaccessible precision, and enable molecular devices with advanced functionalities.[2–4] As examples, ultrathin organic layers with appropriate molecular-orbital (MO) energies are integrated with other inorganic or organic materials to realize Ohmic contacts for hole injection,[5] and donor/acceptor hetero-interfaces for efficient collection of light-induced charges.[6] Moreover, new semiconductor,[7,8] metal[9] and ferromagnetic materials[10,11] can be discovered by forming controlled interfaces between molecular layers and other materials. For structural control of molecular materials, self-assembly processes and sequential deposition of different molecules have been used, but these approaches do not provide full control of the structure, so the final structure is limited to the spontaneously formed ones.[12]

Ultrathin molecular films with spatially uniform thickness and mechanical robustness can provide an effective resource for use in molecular-level fabrication of artificially engineered structures. Numerous different kinds of molecular films can be stacked layer-by-layer (*L*-by-*L*) to precisely control the thickness and vertical composition of the final films.[13] The ability to separate the growth process from the interface-formation process[14] offers the ability to form heterointerfaces from various combinations of molecules. However, reliable transfer of ultrathin molecular films is still challenging due to their weak mechanical strength,[15] and self-assembled molecular layers have been mostly studied in as-grown states on the growth substrates.[16–18]

Here, we report ultrathin yet mechanically robust molecular building blocks, which can be transferred onto arbitrary surfaces. Monolayer (ML) hexagonal boron nitride (h-BN) grown on copper (Cu) serves as a growth template to facilitate layer-wise growth of organic molecules.[19] The ML h-BN also mechanically supports an ultrathin molecular layer with a minute increment of the total thickness, so the films can be transferred reliably (**Figure 1**a).[20,21] This process realized various molecular building blocks. We discuss how the molecules form uniform film structures on ML h-BN support, and the general requirements for realizing molecular building blocks with the same approach. Finally, we demonstrate *L*-by-*L* assembly to form ultrathin films, including donor/acceptor superlattice films, which have controlled interfaces.

S. Choi, Dr. N. N. Nguyen, S.-J. Yang, Prof. K. Cho, Prof. C.-J. Kim
Department of Chemical Engineering
Pohang University of Science and Technology
Pohang 37673, South Korea
E-mail: kimcj@postech.ac.kr
Y. Lee, Prof. K. Kim
Department of Physics
Yonsei University
Seoul 03722, South Korea
Y. Lee, Prof. K. Kim
Center for Nanomedicine
Institute for Basic Science (IBS)
Seoul 03722, South Korea
Prof. C.-J. Kim
Institute for Convergence Research and Education in Advanced Technology
Yonsei University
Seoul 03722, South Korea
The ORCID identification number(s) for the author(s) of this article can be found under https://doi.org/10.1002/admi.202000522.

DOI: 10.1002/admi.202000522

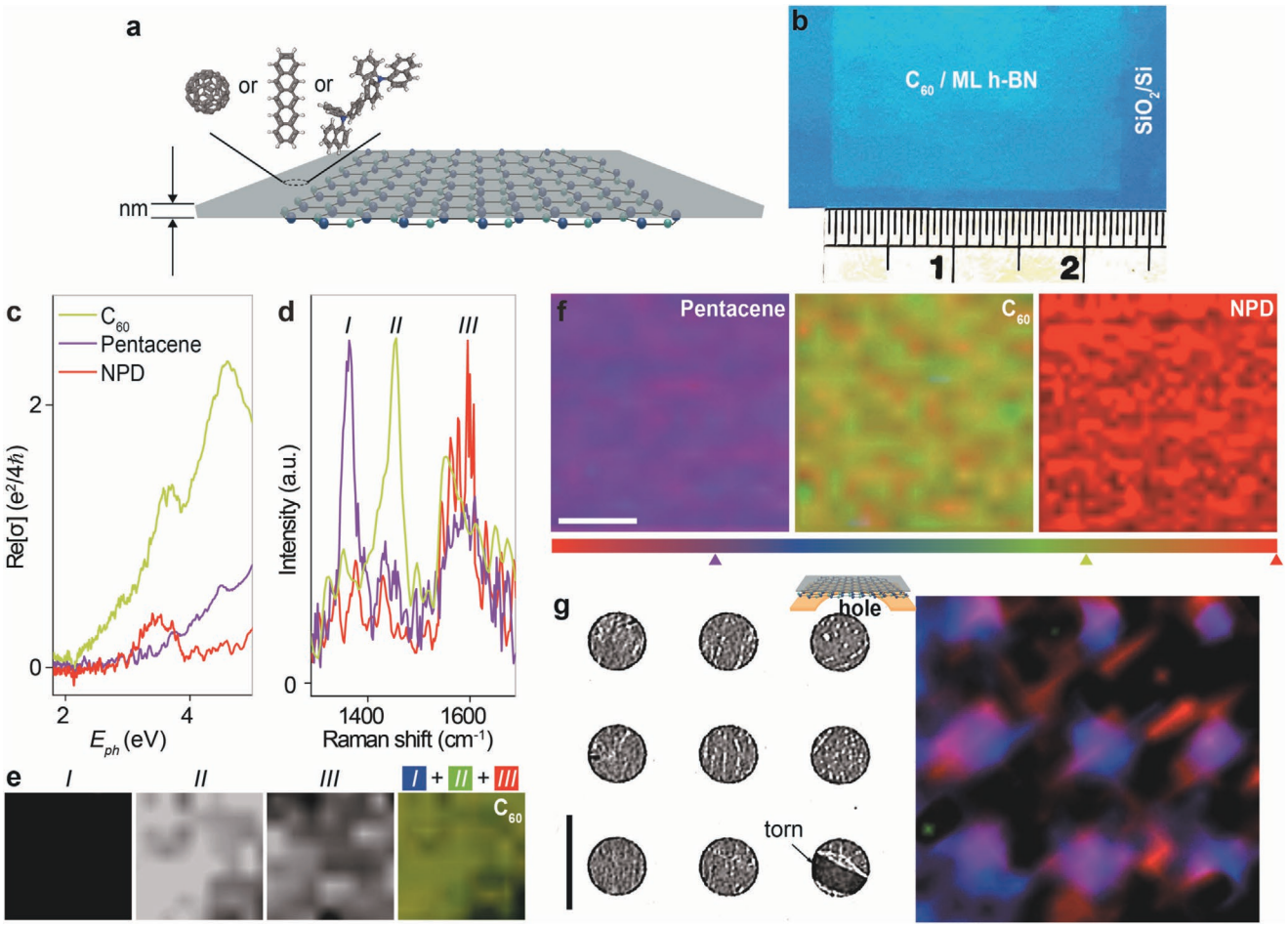

Figure 1. Transferrable molecular building blocks with uniform nanometer thickness. a) Schematic of various ultrathin organic films (C_{60}, pentacene, or NPD) on ML h-BN. b) Optical image of a transferred C_{60}/ML h-BN film on a SiO_2/Si substrate, taken through an optical bandpass filter (central wavelength: 450 nm, full width at half maximum: 40 nm) to maximize the contrast (ruler scale: cm). c) Real part of optical conductivity spectra of molecule/ML h-BN films. d) Raman spectra by an excitation wavelength of 532 nm. e) Customized color scheme to generate Raman intensity maps. Intensity maps are obtained at three wavenumbers, where the strongest intramolecular vibration peaks for each molecules are observed (I: pentacene; II: C_{60}; III: NPD), then combined after colorizing to I: blue; II: green; III: red. As an example, C_{60} with Raman intensities at both II and III energies shows a light green color as a mixture of green and red. f) Color-coded Raman maps for pentacene, C_{60}, and NPD (scale bar: 5 μm). The triangular marks at the bottom color scale indicate the expected color for pentacene, C_{60}, and NPD, respectively. g) Contrast-inverted TEM image (left) and color-coded Raman map (right) of ultrathin pentacene/ML h-BN film transferred onto a TEM grid with holes (scale bar: 2 μm). For the Raman map, pentacene molecules are selected, because its peak energy is distinct from the background signals of amorphous carbon in the grid.

2. Results and Discussion

2.1. Transfer-Compatible Molecular Building Blocks

Ultrathin building block layers composed of molecule *X* (*X*: C_{60}, pentacene, or *N*,*N*′-di(1-naphthyl)-*N*,*N*′-diphenyl-(1,1′-biphenyl)-4,4′-diamine (NPD)) and ML h-BN layer are demonstrated. These molecules have distinct MO energies (Figure 1).[22] Pentacene is a representative electron donor that has low ionization energy (4.9 eV). C_{60} is a representative electron acceptor that has high electron affinity (4.5 eV). NPD is often used as a hole-transport layer, due to its wide band gap (3.0 eV) and relatively high ionization energy (5.4 eV). Large-scale films (several square centimeters) of *X*/ML h-BN with nanometer-level thicknesses (Figure S1, Supporting Information) were formed uniformly on arbitrary substrates. As a representative example, the optical image of C_{60}/ML h-BN film on a SiO_2/Si substrate (Figure 1b) has uniform contrast over the whole transferred area, compared to the bare substrate region.[23] Only C_{60} can result in significant optical contrast in the wavelength region of illuminated light (430–470 nm); this result indicates that the formation of molecular films was scalable.

The optical absorption and Raman spectra of the *X*/ML h-BN films further confirm characteristic features associated with their MO energies and intramolecular vibrations for each molecule (Figure 1c,d). To spatially resolve different molecular species, we generate color-coded Raman maps by colorizing the Raman spectra (Figure 1e). The colored Raman map of each molecular film (Figure 1f) shows uniform color associated with distinct peaks in the Raman spectrum.

Freestanding forms of ultrathin *X*/ML h-BN were constructed to check the mechanical strengths of the films. Films

were suspended over a grid that had an array of 1.2 μm wide holes; the integrity of the films was confirmed by both transmission electron microscopy (TEM) (Figure 1g; left half) and color-coded Raman map (right half), which show uniform signals on the freestanding regions. Together, data in Figure 1 demonstrate that ultrathin molecular building blocks with high spatial homogeneity and mechanical strength were fabricated using various small molecules over large areas. Below, we detail the process of fabricating the molecular films, with C_{60} building block as an example.

2.2. Fabrication of Spatially Uniform Films with Nanoscale Molecular Additives

The fabrication process entails four main steps (**Figure 2**a): i) Growth of ML h-BN on Cu(111) by chemical vapor deposition, ii) Thermal deposition of molecules onto ML h-BN/Cu surface, iii) Postannealing of the sample, and iv) transfer of the composite of molecule/ML h-BN onto arbitrary surfaces. Cu(111) surface enables large-scale growth of ML h-BN, and thermodynamically favors the layer-growth mode for the top molecules, considering the asymmetric binding energies of molecules toward parallel and perpendicular directions to the surface.[24] C_{60} molecules bind more strongly to h-BN bulk crystal (binding energy of 2.3 eV) than to other C_{60} molecules (1.6 eV) without inducing considerable strain energy, due to the softness of the film.[25,26] Here, C_{60} is expected to bind even more strongly than expected to ML h-BN/Cu, because C_{60} can remotely interact with the underlying Cu by efficient charge transfer through a one-atom-thick barrier.[27] As a result, this method can achieve full surface coverage of molecules with a nominal monolayer thickness.

All the tested molecules that formed layers that had an average thickness close to one monolayer showed discrete islands in the as-grown state; postannealing at 220 °C transformed them to a spatially uniform film, which is the thermodynamically preferred structures (Figure 2 for C_{60}, Figures S1 and S2 in the Supporting Information for pentacene and NPD). After the deposition step (ii), C_{60} forms a rough surface (Figure 2b; top), in which C_{60} islands of several tens of

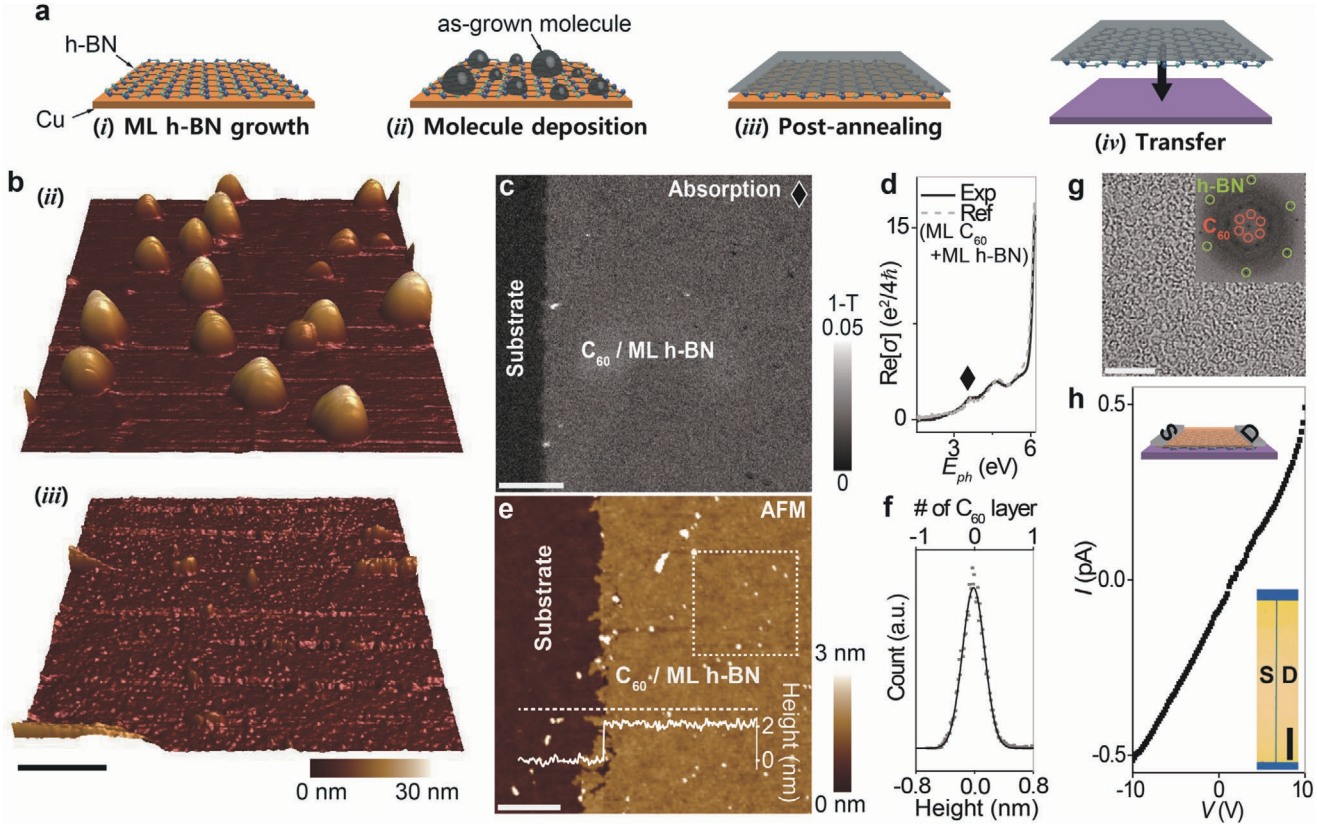

Figure 2. Fabrication of spatially uniform films with nanoscale molecular additives. a) Schematic of processes to fabricate transferrable ultrathin film with molecular additives. b) AFM images of C_{60}/ML h-BN/Cu film after the step (ii) (top) and (iii) (bottom) in (a) (scale bar: 200 nm). c) Absorption contrast image of C_{60}/ML h-BN film on a fused silica substrate at 3.62 eV photon energy, as marked in (d) (scale bar: 20 nm). d) Real part of optical conductivity spectra (solid line) of C_{60}/ML h-BN film measured by a light spot of 1 mm in diameter; the result is identical to the sum of the previously reported optical conductivities (dotted line) of ML C_{60} and ML h-BN. e) AFM height image of transferred C_{60}/ML h-BN on SiO_2/Si with the height profile along the dotted line across the edge of the film (scale bar: 1 μm). f) Height histogram over the dotted square area in (e), showing thickness variation less than an ML C_{60} thickness. g) High-resolution TEM image (main) and fast Fourier transform image (inset) from a freestanding C_{60}/ML h-BN film (scale bar: 5 nm). Diffraction patterns from h-BN (green) and C_{60} (orange) arrays, h) Two-terminal current–voltage (I–V) curves for C_{60}/ML h-BN channel. Insets: a scheme and an optical image of the device (scale bar: 100 μm).

nanometers in thickness are sparsely located with a surface coverage of ≈10%. The nominal film thickness on the whole surface area is estimated to be 0.8 nm, which is equivalent to the thickness of monolayer C_{60} film.[26] After postannealing (iii), the surface (Figure 2b; bottom) becomes smooth with noticeable reduction of C_{60} agglomeration.

Along with the morphological change, the amount of C_{60} was measured by optical absorption in films transferred onto fused silica substrates. Both as-deposited and postannealed C_{60} samples showed the same spectral intensities (Figure S3, Supporting Information) that match with the sum of reported absorption spectra for ML h-BN and ML C_{60} film (Figure 2d);[19,28] this result indicates that the postannealing process does not cause sublimation of C_{60} molecules. Moreover, an optical absorption image (Figure 2c) of the film at one of the peak energies (Figure 2d; diamond symbol) associated with C_{60} excitons shows a uniform value, that is equivalent to that of ML C_{60}, across the film area.

The uniform microstructure of the film was confirmed by atomic force microscopy (AFM) and transmission electron microscopy (TEM). Over the whole scanned area, the thickness of transferred films near the edge (Figure 2e) was homogenously ≈2 nm, which is close to the sum of the effective thicknesses of ML h-BN (0.33 nm) and two ML C_{60} (0.8 nm) measured in their bulk counterparts; the discrepancy with the average ML thickness of C_{60} measured in Figure 2d might be related to reconstructed structure of the C_{60} film by the interaction with the underlying surface. The TEM characterizations confirm the existence of closely packed ultrathin C_{60} domains (1–2 ML) by atom-scale images (Figure 2g; main) and diffraction pattern (inset). The continuity of the film was further confirmed by electrical transport measurements using two-point contacts across the C_{60}/ML h-BN film (Figure 2h). The measured conductivity of the film was 2.45×10^{-9} S cm^{-1}, whereas ML h-BN without a C_{60} superlayer showed no detectable conduction ($<5 \times 10^{-11}$ S cm^{-1}); the difference indicates the presence of conductance pathways within the C_{60} film.

2.3. Growth Dynamics of Molecular Films

The morphology of molecular islands in the as-grown state is contradictory to the thermodynamic prediction. Therefore, the morphology must have been determined by a kinetically limited growth in a highly nonequilibrium growth condition.[29] Specifically, after C_{60} nuclei form on the ML h-BN/Cu surface, the molecules accumulate much faster on the surfaces of C_{60} nuclei (**Figure 3**a) than on the bare ML h-BN/Cu surface (Figure 3b), developing prominent islands in the as-grown state (Figure 2b; top). The molecular deposition rate is kept extremely small in our growth condition to enable precise control of the total amount of deposited C_{60}. With the low deposition rate, the nucleation mostly happened along the step edges of Cu(111) surface, starting in the early stage of the growth (Figure 3c). After this nucleation, the C_{60} nucleus thickened quickly at ≈2.5 nm min^{-1}, as confirmed by AFM (Figure 3a,d). However, noticeable domains took much longer to form on the ML h-BN/Cu surface (Figure 3b,d), and they grew at ≈0.072 nm min^{-1},

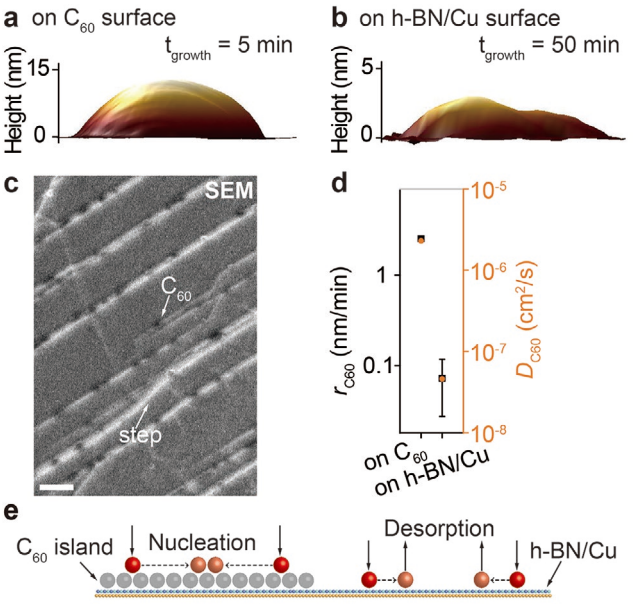

Figure 3. Surface sensitive growth rate of C_{60}. Cross views of 3D AFM height images of C_{60} clusters grown on a) pre-existing C_{60} surface for 5 min and b) ML h-BN/Cu surface for 50 min. c) SEM image of as-deposited C_{60} molecules on ML h-BN/Cu (scale bar: 100 nm). d) Growth rate r_{C60} and surface diffusivity D_{C60} of C_{60} on each surface. e) Schematic of surface-sensitive nucleation processes.

which is about 1/35 as fast as on C_{60} surfaces. All of the molecules tested showed higher growth rate on the molecular surface than on the h-BN.

The different growth rates originate from surface-dependent nucleation rates (Figure 3e). During the incomplete condensation regime with a low deposition rate, most of surface-adsorbed molecules re-evaporate without forming a stable cluster that has a size greater than the critical radius for nucleation.[29] Therefore, the nucleation process is the growth-rate-limiting step, especially in the early stages of growth. The nucleation rate increases with an increase in the mean diffusion distance $\lambda_d = \sqrt{D \cdot \tau_A}$ of ad-molecules, where D [cm^2 s^{-1}] is the surface diffusivity and τ_A [s] is the residual time of the ad-molecules.[30] The C_{60} molecules are expected to have higher D and lower λ_d on the surface of C_{60} domains than on the ML h-BN/Cu surface, because the intermolecular interactions between C_{60} ad-molecules and surface of C_{60} domains are weaker than between C_{60} ad-molecules and ML h-BN/Cu, so both surface diffusion and desorption of C_{60} are easier on C_{60} domains than on h-BN/Cu. Considering the two conflicting effects, our observation suggests that the local surface interaction changes D more significantly than λ_d, so nucleation rate increases on the C_{60} surface. Indeed, considerably higher D is reported on the C_{60} surface than on the ML h-BN/Cu (Figure 3d; right y-axis).[31] The phenomenon is consistent with a previous comparison of molecular nucleation on organic versus inorganic surfaces.[30] In the incomplete-condensation regime, we expect this highly surface-selective growth rate to happen universally for most small molecules that have surface that allow faster D of ad-molecules than does the ML h-BN/Cu surface.

Kinetically driven molecular islands can be feasibly transformed to a thermodynamically favorable form by postannealing, if the process provides a sufficient thermal energy for diffusion.[32,33] For C_{60} molecules of nominal ML thickness on ML h-BN/Cu, we found that an annealing temperature > 490 K can yield a uniform film with a full coverage in <60 min. This temperature is significantly lower than the sublimation temperature of 700 K in low vacuum,[34] so annealing does not eject molecules. The reaction rate is proportional to $\exp(-\Delta E_B/(k_B T))$, where ΔE_B is the potential energy barrier, $k_B = 8.617 \times 10^{-5}$ eV K^{-1} is the Boltzmann constant, and T [K] is the process temperature. The efficient molecular diffusion without desorption indicates that ΔE_B for diffusion is lower than for desorption.

The diffusion-limiting step to determine ΔE_B is identified by observing the morphological evolution during annealing. As an example, during annealing at 470 K for 60 min, the thick as-grown domains (**Figure 4**a; left) smoothed to a reduced height and wider lateral size (Figure 4a; right), but the process does not result in a full surface coverage. The islands were still higher more than five C_{60} layers thick in most of the region with stiff edges; this result indicates that molecular wetting was incomplete; i.e., that both intra- and interlayer molecular diffusions occur within the multilayer C_{60} island in an asymmetric fashion, whereas the diffusion from C_{60} surface to ML h-BN/Cu at the edge front is limited by a Ehrlich–Schwoebel barrier.[30] Also, the morphological evolution during annealing is highly sensitive to the surface material. On a fused silica substrate, as-grown C_{60} islands (Figure 4b; top) did not change to a film structure after the same annealing condition (Figure 4b; bottom); this difference in result demonstrates that the interaction between molecules and the substrate determines the most stable structure.

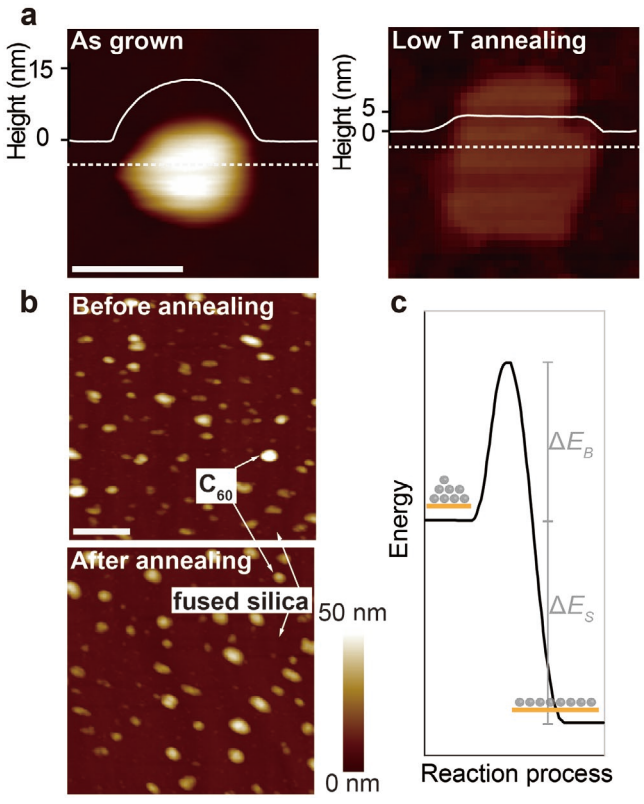

Figure 4. Postannealing effect on the morphology of as-grown C_{60} clusters. a) AFM height images of a C_{60} molecular cluster before (left) and after postannealing at 200 °C for 60 min (right). The white lines indicate the height profiles along the dotted lines across the clusters. b) AFM height images of C_{60} molecules on fused silica substrates before (top) and after postannealing (bottom) (scale bar: 1 μm). c) Potential energy profile of the morphological change reaction of molecules. ΔE_B and ΔE_S represent the potential energy barrier for the molecular wetting on ML h-BN/Cu from a cluster structure and the molecular free energy difference between in an island structure and in a film structure, respectively.

The feasibility of making an ultrathin film with other molecular additives can be expected by considering both ΔE_B and the free-energy difference ΔE_S between molecules in an island structure and molecules in a film structure (Figure 4c). Various small molecules can interact strongly with the ML h-BN/Cu surface to promote a layer-growth mode, yet highly nonuniform islands can be formed and maintained by the surface-dependent barriers to nucleation and diffusion in a kinetically driven growth regime. If ΔE_S is significantly higher than ΔE_B, then thermal energy comparable to ΔE_B yields reactions that change asymmetric morphology toward the most-stable film structure. Therefore, our process to produce ultrathin molecular building blocks should use molecules that have low ΔE_B.

Our process can be applicable to many small-molecules, due to two factors. First, small molecules generally have high surface diffusivity with low ΔE_B. Second, as the intermolecular interactions are usually weak, it is possible to promote molecular adhesion to ML h-BN/Cu surface with high ΔE_S. While experiments with other molecules are required to further demonstrate the versatility of our process, the method is promising to make ultrathin films with small molecules.

2.4. Layer-by-Layer Assembly of Molecular Building Blocks

Finally, designed materials that use ultrathin molecular building blocks were obtained by laminar *L*-by-*L* assembly (**Figure 5**a). Individual building blocks (Figure 1a) were transferred onto a target substrate sequentially to fabricate ultrathin films (Experimental Section) that have thickness and composition that are controlled at the molecular scale in the vertical direction. As examples, three kinds of films composed of different repeating units were fabricated: two homomolecular building blocks (C_{60}/ML h-BN; pentacene/ML h-BN) and one hetero-molecular building blocks (C_{60}/ML h-BN/pentacene/ML h-BN).

We first present ultrathin homo-molecular films with precisely controlled thicknesses and high spatial uniformity (Figure 5b–d). Multilayer C_{60}/ML h-BN films showed optical conductivity spectra that increase linearly in intensity with increase in the number n of transfers of the repeating units; this result demonstrates successful *L*-by-*L* assembly to control the total number of molecular building blocks (Figure 5b). The molecular structures were also preserved, as confirmed by spatially uniform optical absorption (Figure 5b; right) and AFM height images (Figure 5c) of the multilayer films with different n. For every "C_{60}/ML h-BN" unit, the total thickness of the film increased by 2.05 nm (Figure 5c,d; orange), which is close to the thickness of a single layer (Figure 2); this similarity indicates

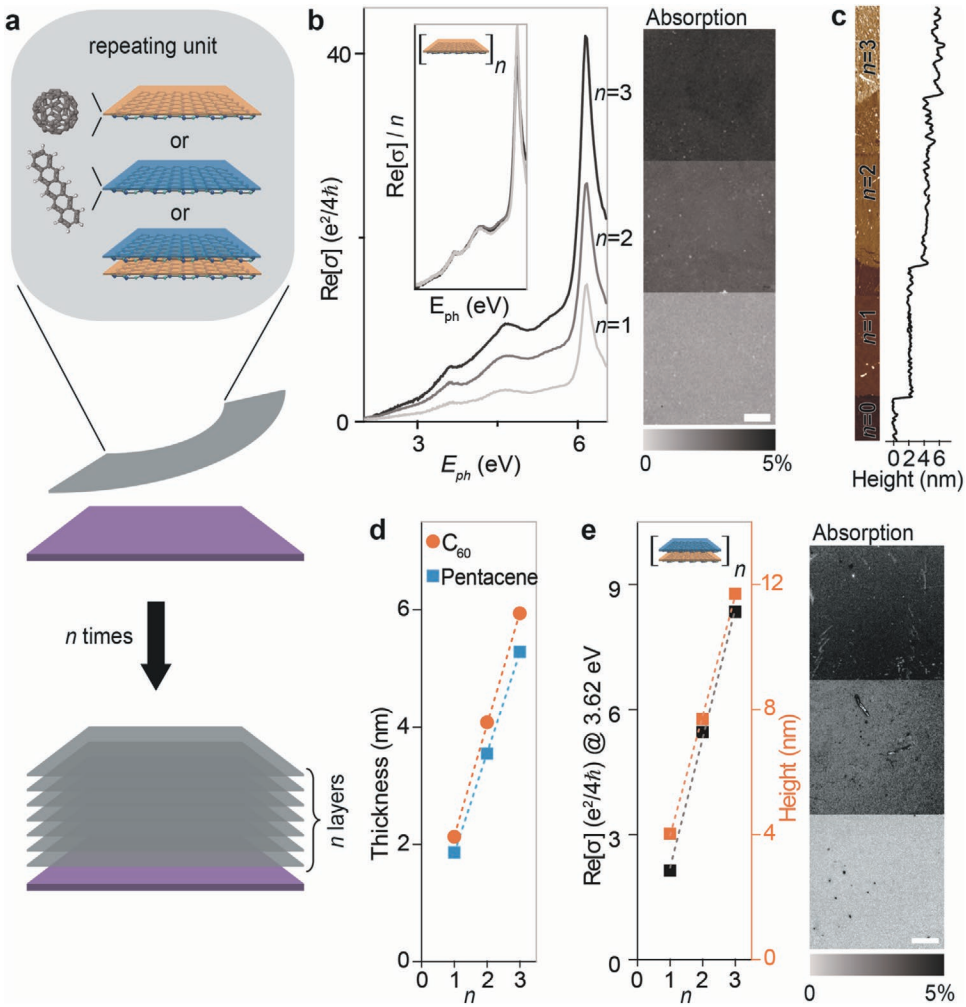

Figure 5. *L*-by-*L* assembly of ultrathin molecular building blocks. a) Schematic of *L*-by-*L* assembly of building block units (ex. C_{60}/ML h-BN, pentacene/ML h-BN, C_{60}/ML h-BN/pentacene/ML h-BN). b) Real part of optical conductivity spectra (left) and optical absorption images obtained at 3.35 eV (right) of films of [unit]n fabricated by the number *n* of transfers of the repeating units. In the inset, the spectra are normalized by *n* (scale bar: 100 μm). c) AFM height image (left) and cross-sectional height profile across the boundaries of the regions with different *n*. d) Thickness of films of [unit]n (unit: C_{60}/ML h-BN, pentacene/ML h-BN). e) Optical conductivity measured at 3.62 eV and height of films of [C_{60}/ML h-BN/pentacene/ML h-BN]n (left) and optical absorption images obtained at 3.35 eV for each film (right) (scale bar: 50 μm).

that no additional impurities are introduced at the interfaces between building blocks during the repeated transfer process, so total thickness can be controlled precisely. The approach can be applied to other molecular building blocks such as pentacene (Figure 5d; blue) to fabricate films with precisely determined thickness by controlling *n*.

Different molecular building blocks can be assembled together to form structures that have engineered hetero-interfaces. As an example, one can build donor-acceptor superlattice by alternately transferring C_{60}/ML h-BN and pentacene/ML h-BN building blocks. The final film shows uniform optical properties and height defined by *n* repeats of the unit of C_{60}/ML h-BN/pentacene/ML h-BN composite (Figure 5e, Figure S4, Supporting Information). ML h-BN supports are atomically thin, so interlayer interactions including charge transfer phenomena are expected to remain efficient between the dissimilar molecular building blocks, and therefore to facilitate realization of advanced functional elements with various other molecules.[2,35]

3. Conclusion

We have reported a versatile and scalable approach to form transfer-compatible ultrathin building blocks composed of various small molecules. These building blocks can be assembled into artificial structures that have pristine van der Waals interfaces. We find that atomically thin ML h-BN film can serve as both a mechanical support for transfer, and as a growth substrate for uniform film growth of various small molecules. The approach allows combination of molecular building blocks with pre-existing material systems. The hybrid materials would exploit the advantages of both building blocks to provide advanced functionality, and would open opportunities to discover new properties that arise from the interplay between them. For example, when small molecules with complex geometry and various functional groups are combined with 2D materials that have excellent electrical and optical properties, the composites can be utilized in smart devices that have high

selectivity and good (opto-)electrical properties.[36–38] Also, the hybrid system poses an interesting question of how the physiochemical properties of molecules change when they interact with other materials.[39] Our work offers a useful route to explore the question.

4. Experimental Section

Growth of ML h-BN Film: ML h-BN film was grown by chemical vapor deposition on Cu foil (Nilaco corporation, #CU-113213, 30 μm thick, 99.9% purity). First, the Cu foil was annealed at 1030 °C for 4 h under flow of H_2 at 70 sccm with a total pressure of 5 Torr; then ML h-BN film was grown at 1040 °C for 30 min by additionally introducing a borazine precursor (Gelest, #INBO009, kept at −20 °C) in Ar carrier gas at 0.15 sccm. During the cooling process after growth, the borazine injection was maintained until the film had cooled to 600 °C, then only H_2 was introduced until the temperature reached < 200 °C to allow unloading of the sample.

Fabrication of Spatially Uniform Nanoscale Molecular Additives: All of the tested molecules were deposited by thermal evaporation at the high vacuum condition (1.0×10^{-8} Torr) onto ML h-BN/Cu surface at a rate of 0.1 Å s^{-1}. The substrate temperatures during the deposition were 170, 110, and 125 °C for C_{60}, pentacene, and NPD, respectively. For the postannealing process, the C_{60}, pentacene, and NPD samples were re-loaded into an annealing chamber, then annealed at 220, 110, 125 °C, respectively in Ar atmosphere of 5 Torr with evacuation for 1 h.

Transfer of Molecular Building Blocks: To isolate the molecular building blocks, the molecule/ML h-BN/Cu foil was floated on a Cu etchant of $FeCl_3$ aqueous solution (Sigma-Aldrich, #667528) for 20 min without introducing any additional supporting layer. After complete etching of Cu, the molecule/ML h-BN film was transferred onto a surface of ultrahigh purity deionized water by scooping with a SiO_x substrate, then and releasing the ultrathin film. The process was repeated twice in a clean water to rinse the surface, then the film was transferred onto a target substrate by the same method.

Optical Characterization: For optical spectroscopy and imaging, we used a home-built hyperspectral imaging set-up in which wavelength-tunable light from a Xenon lamp and a monochromator were introduced into a lens-free optical microscope to minimize chromatic aberration.[23]

TEM Characterization: TEM images were acquired using a double Cs-aberration corrected JEOL ARM-200F operated at 80 kV.

Supporting Information

Supporting Information is available from the Wiley Online Library or from the author.

Acknowledgements

This research was supported by the International Research & Development Program (NRF-2017K1A3A1A12073407) and the Creative Materials Discovery Program (NRF-2018M3D1A1058793) of the National Research Foundation of Korea (NRF) funded by the Ministry of Science, ICT & Future Planning, as well as the Basic Science Research Program through the NRF funded by the Ministry of Education (NRF-2017R1D1A1B03034896). Y.L. and K.K. acknowledge support from the Institute for Basic Science (IBS-R026-D1). This article was amended on May 19, 2020 to correct the first name of Kwanpyo Kim.

Conflict of Interest

The authors declare no conflict of interest.

Keywords

layer-by-layer assembly, molecular building blocks, organic heterostructure, transfer, ultrathin films

Received: March 24, 2020
Revised: April 20, 2020
Published online: May 12, 2020

[1] N. Koch, *ChemPhysChem* **2007**, *8*, 1438.
[2] M. Oehzelt, K. Akaike, N. Koch, G. Heimel, *Sci. Adv.* **2015**, *1*, e1501127.
[3] Y. Zhang, M. Heiranian, B. Janicek, Z. Budrikis, S. Zapperi, P. Y. Huang, H. T. Johnson, N. R. Aluru, J. W. Lyding, N. Mason, *Nano Lett.* **2018**, *18*, 2098.
[4] D. K. Bediako, M. Rezaee, H. Yoo, D. T. Larson, S. Y. F. Zhao, T. Taniguchi, K. Watanabe, T. L. Brower-Thomas, E. Kaxiras, P. Kim, *Nature* **2018**, *558*, 425.
[5] N. B. Kotadiya, H. Lu, A. Mondal, Y. Ie, D. Andrienko, P. W. M. Blom, G. J. A. H. Wetzelaer, *Nat. Mater.* **2018**, *17*, 329.
[6] K. Vandewal, S. Albrecht, E. T. Hoke, K. R. Graham, J. Widmer, J. D. Douglas, M. Schubert, W. R. Mateker, J. T. Bloking, G. F. Burkhard, A. Sellinger, J. M. J. Fréchet, A. Amassian, M. K. Riede, M. D. McGehee, D. Neher, A. Salleo, *Nat. Mater.* **2014**, *13*, 63.
[7] B. Choi, J. Yu, D. W. Paley, M. T. Trinh, M. V. Paley, J. M. Karch, A. C. Crowther, C. H. Lee, R. A. Lalancette, X. Zhu, P. Kim, M. L. Steigerwald, C. Nuckolls, X. Roy, *Nano Lett.* **2016**, *16*, 1445.
[8] H. Zhu, C. Xiao, H. Cheng, F. Grote, X. Zhang, T. Yao, Z. Li, C. Wang, S. Wei, Y. Lei, Y. Xie, *Nat. Commun.* **2014**, *5*, 3960.
[9] H. Alves, A. S. Molinari, H. Xie, A. F. Morpurgo, *Nat. Mater.* **2008**, *7*, 574.
[10] X. Roy, C. H. Lee, A. C. Crowther, C. L. Schenck, T. Besara, R. A. Lalancette, T. Siegrist, P. W. Stephens, L. E. Brus, P. Kim, M. L. Steigerwald, C. Nuckolls, *Science* **2013**, *341*, 157.
[11] F. Al Ma'Mari, T. Moorsom, G. Teobaldi, W. Deacon, T. Prokscha, H. Luetkens, S. Lee, G. E. Sterbinsky, D. A. Arena, D. A. Maclaren, M. Flokstra, M. Ali, M. C. Wheeler, G. Burnell, B. J. Hickey, O. Cespedes, *Nature* **2015**, *524*, 69.
[12] A. Hinderhofer, F. Schreiber, *ChemPhysChem* **2012**, *13*, 628.
[13] J. J. Richardson, M. Björnmalm, F. Caruso, *Science* **2015**, *348*, aaa2491.
[14] S. J. Noever, M. Eder, F. del Giudice, J. Martin, F. X. Werkmeister, S. Hallwig, S. Fischer, O. Seeck, N.-E. Weber, C. Liewald, F. Keilmann, A. Turchanin, B. Nickel, *Adv. Mater.* **2017**, *29*, 1606283.
[15] H. W. Kroto, A. W. Allaf, S. P. Balm, *Chem. Rev.* **1991**, *91*, 1213.
[16] L. Sánchez, R. Otero, J. M. Gallego, R. Miranda, N. Martin, *Chem. Rev.* **2009**, *109*, 2081.
[17] D. He, Y. Zhang, Q. Wu, R. Xu, H. Nan, J. Liu, J. Yao, Z. Wang, S. Yuan, Y. Li, Y. Shi, J. Wang, Z. Ni, L. He, F. Miao, F. Song, H. Xu, K. Watanabe, T. Taniguchi, J. Bin Xu, X. Wang, *Nat. Commun.* **2014**, *5*, 5162.
[18] L. Jiang, H. Dong, Q. Meng, H. Li, M. He, Z. Wei, Y. He, W. Hu, *Adv. Mater.* **2011**, *23*, 2059.
[19] C. J. Kim, L. Brown, M. W. Graham, R. Hovden, R. W. Havener, P. L. McEuen, D. A. Muller, J. Park, *Nano Lett.* **2013**, *13*, 5660.
[20] Y. Kobayashi, K. Kumakura, T. Akasaka, T. Makimoto, *Nature* **2012**, *484*, 223.
[21] M. Kratzer, A. Matkovic, C. Teichert, *J. Phys. D: Appl. Phys.* **2019**, *52*, 383001.
[22] H. Dong, H. Zhu, Q. Meng, X. Gong, W. Hu, *Chem. Soc. Rev.* **2012**, *41*, 1754.
[23] R. W. Havener, C. J. Kim, L. Brown, J. W. Kevek, J. D. Sleppy, P. L. McEuen, J. Park, *Nano Lett.* **2013**, *13*, 3942.
[24] M. H. Grabow, G. H. Gilmer, *Surf. Sci.* **1988**, *194*, 333.

[25] P. Reinke, H. Feldermann, P. Oelhafen, *J. Chem. Phys.* **2003**, *119*, 12547.
[26] G. Dresselhaus, M. S. Dresselhaus, P. C. Eklund, *Science of Fullerenes and Carbon Nanotubes*, Academic Press, San Diego, United States **1996**.
[27] J. Rafiee, X. Mi, H. Gullapalli, A. V Thomas, F. Yavari, Y. Shi, P. M. Ajayan, N. A. Koratkar, *Nat. Mater.* **2012**, *11*, 217.
[28] S. L. Ren, Y. Wang, A. M. Rao, E. McRae, J. M. Holden, T. Hager, K. A. Wang, W. T. Lee, H. F. Ni, J. Selegue, P. C. Eklund, *Appl. Phys. Lett.* **1991**, *59*, 2678.
[29] J. A. Venables, G. D. T. Spiller, M. Hanbucken, *Rep. Prog. Phys.* **1984**, *47*, 399.
[30] S. Pratontep, F. Nüesch, L. Zuppiroli, M. Brinkmann, *Phys. Rev. B* **2005**, *72*, 085211.
[31] J. A. Venables, in *Growth Properties of Ultrathin Epitaxial Layers*, Vol. *2* (Eds: D. A. King, D. P. Woodruff), Elsevier Science B.V., Amsterdam, the Netherlands **1997**, Ch.1.
[32] B. Krause, A. C. Dürr, F. Schreiber, H. Dosch, O. H. Seeck, *Surf. Sci.* **2004**, *572*, 385.
[33] S. Bommel, H. Spranger, C. Weber, N. Kleppmann, S. V. Roth, S. H. L. Klapp, S. Kowarik, *Phys. Status Solidi RRL* **2015**, *9*, 646.
[34] C. Pan, M. P. Sampson, Y. Chai, R. H. Hauge, J. L. Margrave, *J. Phys. Chem.* **1991**, *95*, 2944.
[35] S. Verlaak, D. Beljonne, D. Cheyns, C. Rolin, M. Linares, F. Castet, J. Cornil, P. Heremans, *Adv. Funct. Mater.* **2009**, *19*, 3809.
[36] M. Gobbi, S. Bonacchi, J. X. Lian, A. Vercouter, S. Bertolazzi, B. Zyska, M. Timpel, R. Tatti, Y. Olivier, S. Hecht, M. V Nardi, D. Beljonne, E. Orgiu, P. Samorì, *Nat. Commun.* **2018**, *9*, 2661.
[37] J. R. Greer, J. Park, *Nano Lett.* **2018**, *18*, 2187.
[38] D. Jariwala, T. J. Marks, M. C. Hersam, *Nat. Mater.* **2017**, *16*, 170.
[39] R. Mirzayev, K. Mustonen, M. R. A. Monazam, A. Mittelberger, T. J. Pennycook, C. Mangler, T. Susi, J. Kotakoski, J. C. Meyer, *Sci. Adv.* **2017**, *3*, e1700176.